Sustainable Energy & Fuels

ROYAL SOCIETY OF CHEMISTRY

CORRECTION

View Article Online
View Journal | View Issue

Check for updates

Cite this: *Sustainable Energy Fuels*, 2025, **9**, 6563

Correction: Advances and strategies in scalable coating techniques for flexible perovskite solar cells

Hou-Chin Cha, [ab] Shih-Han Huang, [b] Chia-Feng Li,[cd] Feng-Yu Tsai, [d] Wei-Fang Su *[cd] and Yu-Ching Huang *[bcef]

DOI: 10.1039/d5se90082d

rsc.li/sustainable-energy

Correction for 'Advances and strategies in scalable coating techniques for flexible perovskite solar cells' by Hou-Chin Cha *et al.*, *Sustainable Energy Fuels*, 2025, https://doi.org/10.1039/D5SE00873E.

The authors regret that statements acknowledging reproduced work were omitted from a number of the captions of figures (Fig. 1–11, 13) in the original manuscript, including the graphical abstract. The figures containing reproduced work, along with updated captions containing the acknowledgement statements, are displayed in this notice. The references in the captions are as they appear in the original manuscript.

Open Access Article. Published on 31 October 2025. Downloaded on 5/8/2026 2:03:17 PM.
This article is licensed under a Creative Commons Attribution 3.0 Unported Licence.

[a]*College of Engineering, Ming Chi University of Technology, New Taipei City, 24301, Taiwan*
[b]*Organic Electronics Research Center, Ming Chi University of Technology, New Taipei City, 24301, Taiwan. E-mail: huangyc@mail.mcut.edu.tw*
[c]*Department of Materials Engineering, Ming Chi University of Technology, New Taipei City, 24301, Taiwan*
[d]*Department of Materials Science and Engineering, National Taiwan University, Taipei 10617, Taiwan. E-mail: suwf@ntu.edu.tw*
[e]*Center for Sustainability and Energy Technologies, Chang Gung University, Taoyuan, 33302, Taiwan*
[f]*Research Center for Critical Issues, Academia Sinica, Taipei, 115201, Taiwan*

Open Access Article. Published on 31 October 2025. Downloaded on 5/8/2026 2:03:17 PM.
This article is licensed under a Creative Commons Attribution 3.0 Unported Licence.

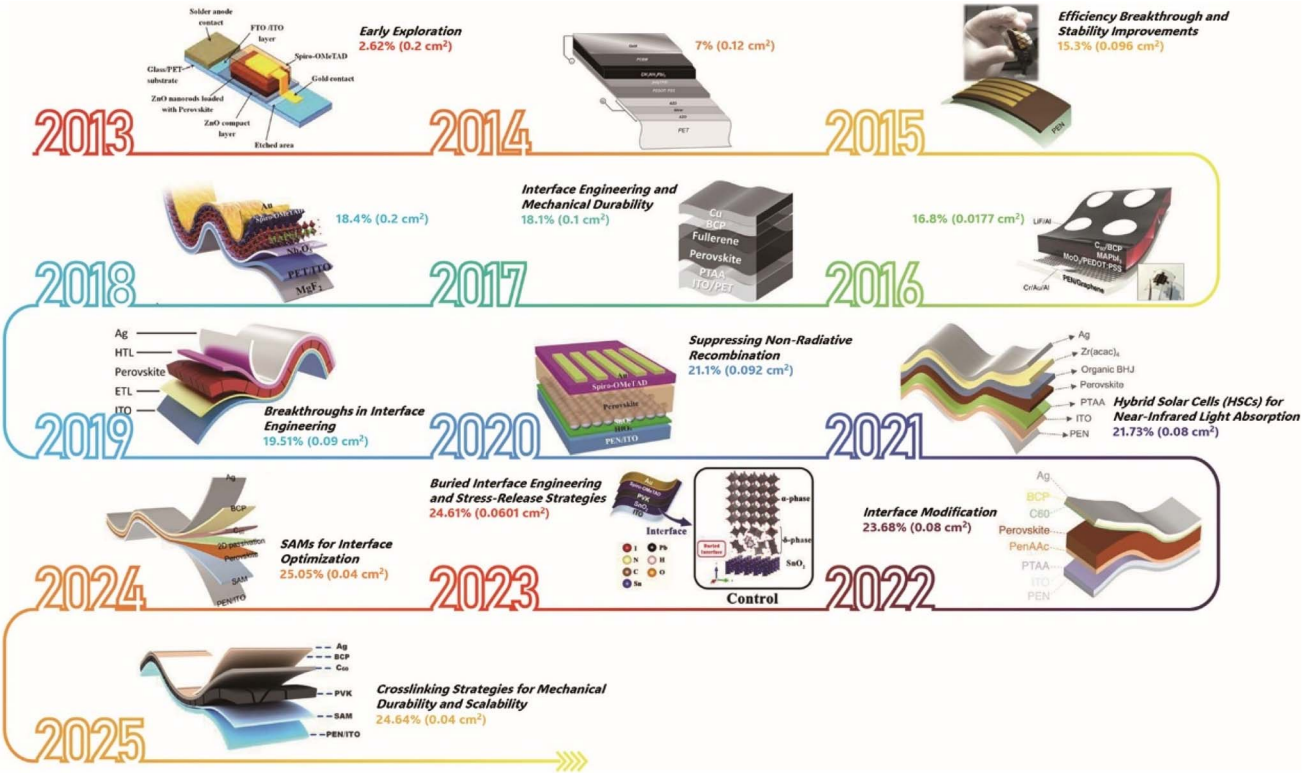

Fig. 1 The progress of power conversion efficiency in flexible perovskite solar cells from 2013 to April 2025.[24–36] (Reproduced from ref. 24, 27, and 31 with permission from the Royal Society of Chemistry; from ref. 28–29 and 32–35 with permission from Wiley-VCH GmbH; from ref. 30 with permission from Wiley; from ref. 26 under CC BY 4.0, *Nature Communications*, 2015; and from ref. 36 under CC BY 4.0, *Science Advances*, 2025.)

This journal is © The Royal Society of Chemistry 2025

Open Access Article. Published on 31 October 2025. Downloaded on 5/8/2026 2:03:17 PM.
This article is licensed under a Creative Commons Attribution 3.0 Unported Licence.

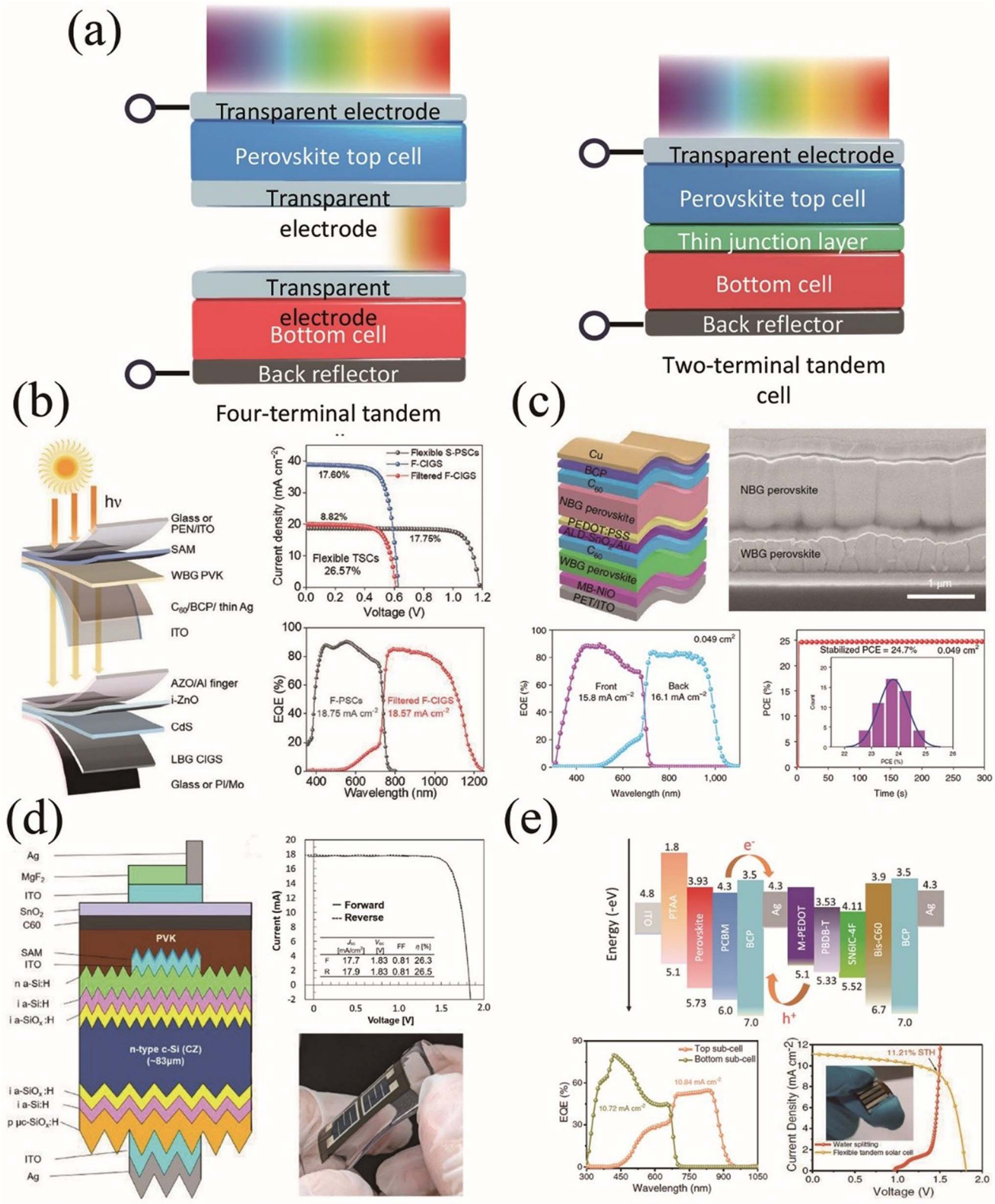

Fig. 2 (a) Schematic illustration of 4-terminal (4T) and 2-terminal (2T) perovskite tandem solar cell (TSC) architectures. (b) Structure of flexible perovskite (PVK)/CIGS 4T TSCs. Shown are the *J*–*V* curves of flexible CIGS (F-CIGS), filtered F-CIGS, and flexible single-junction perovskite solar cells (S-PSCs) with ARP surface modification. Also shown are the EQE spectra of ARP-treated S-PSCs and filtered F-CIGS, with integrated J_{SC} values of 18.75 and 18.57 mA cm^{-2}, respectively.[43] (Reproduced from ref. 43 with permission from Wiley-VCH GmbH.) (c) Device structure and cross-sectional SEM image of a flexible all-perovskite tandem solar cell. The EQE spectra and stabilized power output of the champion flexible tandem cell are shown for a device with an aperture area of 0.049 cm^2.[50] (Reproduced from ref. 50 under CC BY 4.0, *Nature Energy*, 2022.) (d) Schematic diagram and *J*–*V* characteristics of a flexible perovskite/thinned silicon tandem solar cell. Images of the fabricated flexible tandem

device are also shown.[55] (Reproduced from ref. 55 with permission from Wiley.) (e) Energy-level alignment of a 2T perovskite-organic tandem solar cell. EQE spectra of the wide-bandgap perovskite top subcell and low-bandgap OPV bottom subcell are presented, along with the *J*–*V* curve of the flexible tandem device under simulated AM 1.5G illumination. Inset: photograph of the flexible tandem device driving water splitting using NiFe LDH electrodes in a two-electrode configuration.[57] (Reproduced from ref. 57 with permission from Wiley.)

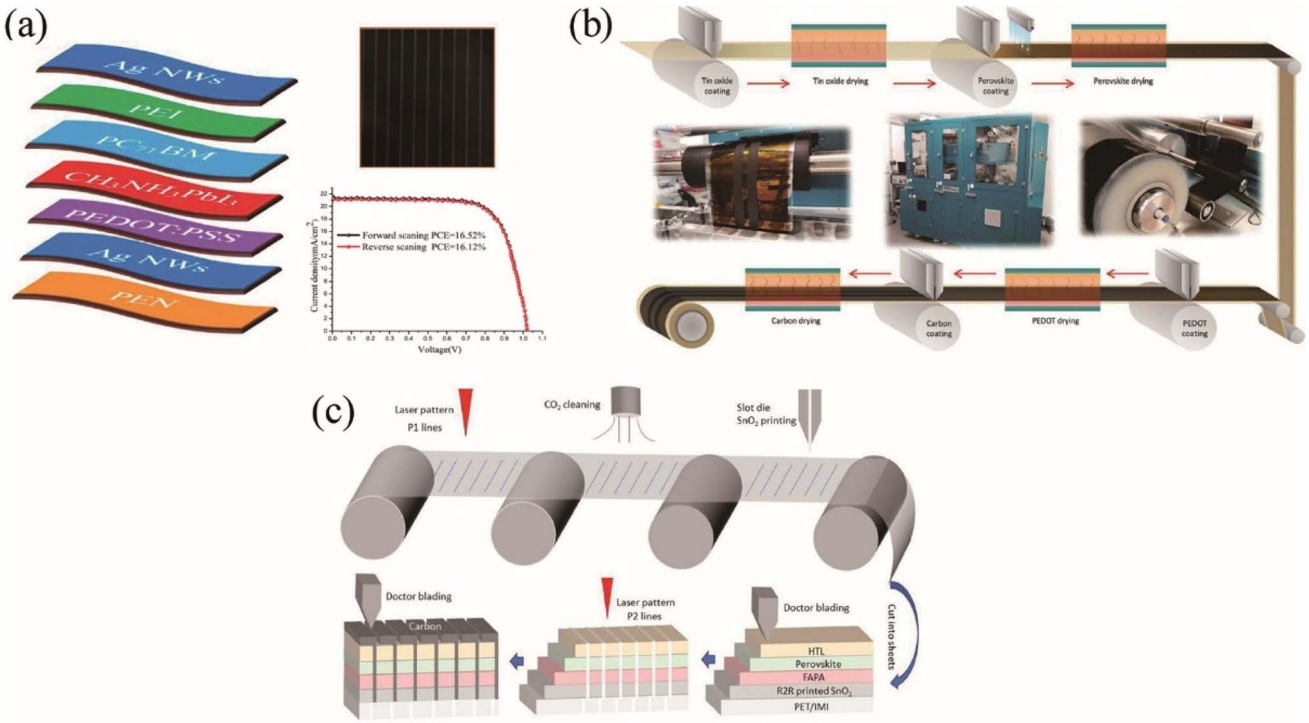

Fig. 3 (a) Structural diagram of the perovskite solar cell architecture. Photograph of a 10 cm × 12 cm perovskite solar cell. Hysteresis characteristics measured at the maximum power point.[58] (Reproduced from ref. 58 with permission from Elsevier.) (b) Schematic illustration of the R2R slot-die coating process used for fabricating perovskite solar cells, featuring a fully printable carbon top electrode.[59] (Reproduced from ref. 59 with permission from Wiley-VCH GmbH.) (c) Workflow for manufacturing F-PSMs, including laser patterning, CO_2 snow-jet cleaning, R2R slot-die coating, doctor blading, and stencil printing. F-PSCs follow a similar process but omit certain laser patterning steps.[60] (Reproduced from ref. 60 with permission from the Royal Society of Chemistry.)

Open Access Article. Published on 31 October 2025. Downloaded on 5/8/2026 2:03:17 PM.
This article is licensed under a Creative Commons Attribution 3.0 Unported Licence.

This journal is © The Royal Society of Chemistry 2025

Open Access Article. Published on 31 October 2025. Downloaded on 5/8/2026 2:03:17 PM.
This article is licensed under a Creative Commons Attribution 3.0 Unported Licence.

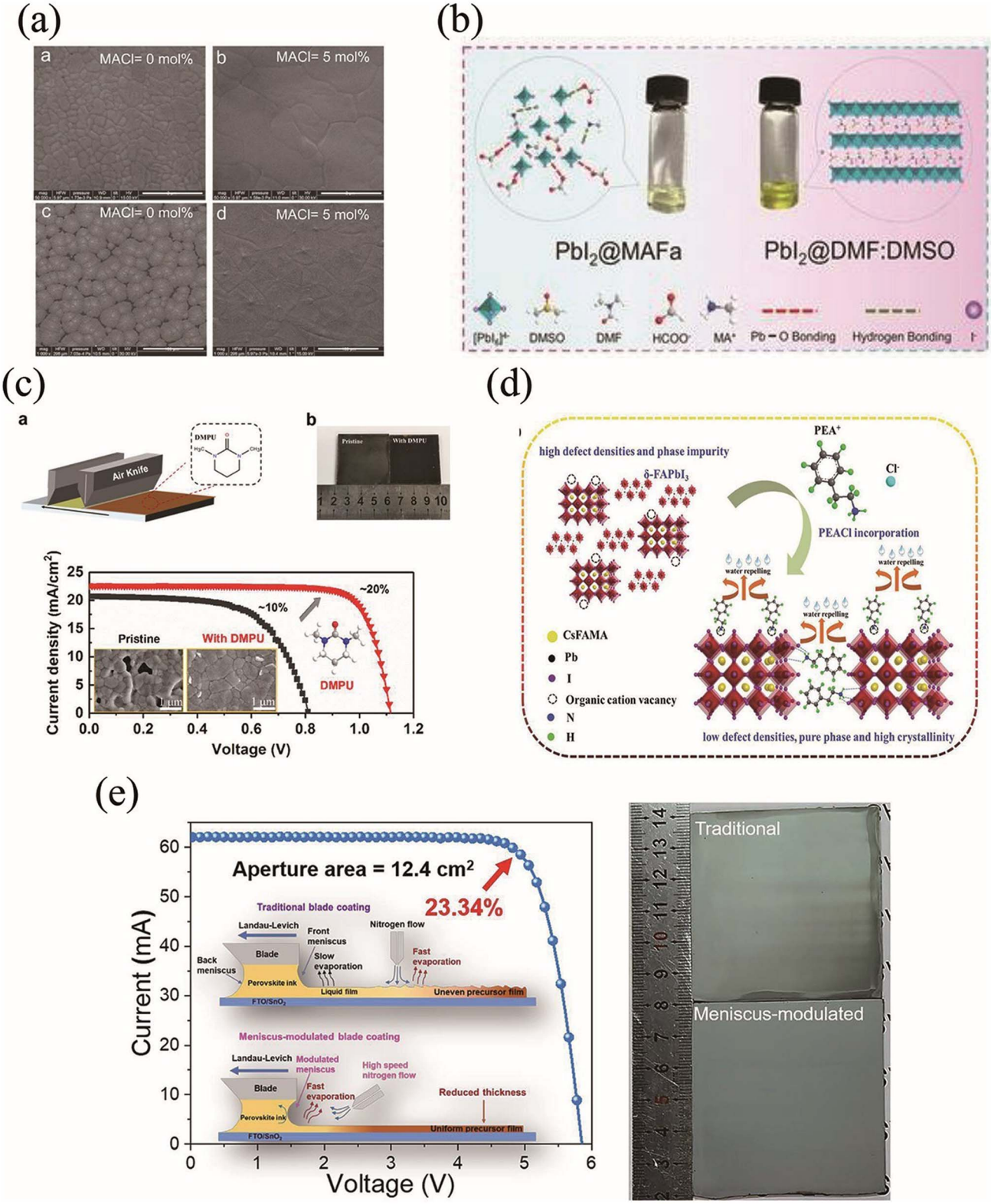

Fig. 4 (a) Morphological comparison of doctor-bladed perovskite films with and without 5 mol% MACl additive. The $MA_{0.6}FA_{0.38}Cs_{0.02}PbI_{2.975}Br_{0.025}$ thin films exhibit significantly improved surface smoothness and grain uniformity upon MACl incorporation. The scale bars are 2 mm and 100 μm, respectively.[62] (Reproduced from ref. 62 with permission from Wiley.) (b) Photographic images of PbI_2@MAFa and PbI_2@DMF:DMSO precursor solutions, accompanied by a schematic diagram illustrating molecular interactions within each solution system. The PbI_2@MAFa solution leads to better crystallization behavior and improved film quality.[68] (Reproduced from ref. 68 under its respective license, *Science*, 2021.) (c) A schematic illustration of the blade coating process used for fabricating FA-dominated perovskite films is presented, alongside the molecular structure of the *N*,*N*′-dimethylpropyleneurea (DMPU) additive. Photographs of the film backsides, with and without

DMPU, highlight the enhancement in film uniformity and coverage achieved through DMPU incorporation.[69] (Reproduced from ref. 69 with permission from the American Chemical Society.) (d) A schematic representation of the effects of PEACl modification is shown, demonstrating the suppression of the non-perovskite δ-phase, effective defect passivation, and improved water repellency. These features collectively enhance device stability and performance.[70] (Reproduced from ref. 70 with permission from Wiley-VCH GmbH.) (e) Comparison between traditional blade coating and the meniscus-modulated blade coating technique. The schematic diagrams highlight key differences in fluid control and film formation. Photographs of 6 cm × 6 cm $FAPbI_3$ films fabricated using both methods clearly show the superior film uniformity achieved *via* the meniscus-modulated approach.[72] (Reproduced from ref. 72 under CC BY 4.0, *Joule*, 2024.)

Open Access Article. Published on 31 October 2025. Downloaded on 5/8/2026 2:03:17 PM.
This article is licensed under a Creative Commons Attribution 3.0 Unported Licence.

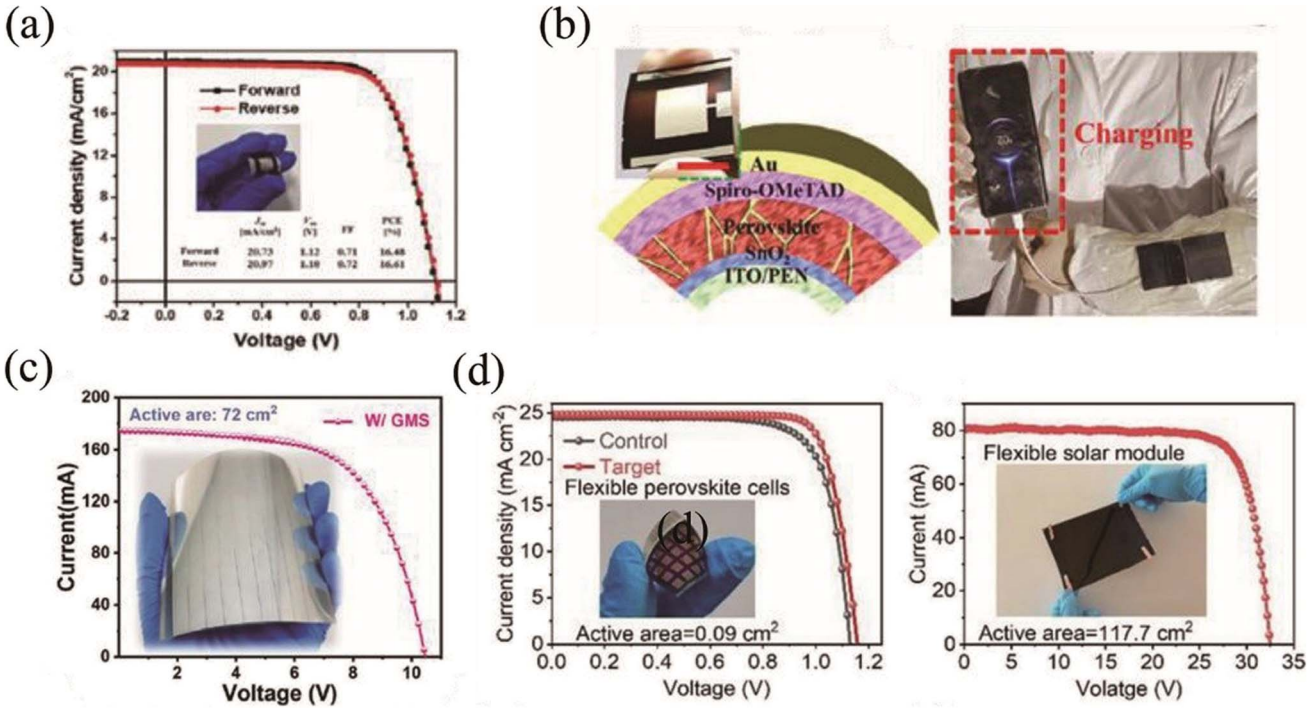

Fig. 5 (a) *J*–*V* curves of large-area F-PSCs (1 cm^2) utilizing a poly(3,4-ethylenedioxythiophene):poly(styrene sulfonate) (PEDOT:PSS, 35 nm)/PTAA bilayer as the hole transport layer. The insets show a photograph of the device and its key performance parameters.[73] (Reproduced from ref. 73 with permission from Wiley.) (b) Schematic illustration of the F-PSC device architecture. The inset displays a photograph of a large-area flexible PSC (scale bar: 1 cm), and additional photos demonstrate its application as a wearable power source.[75] (Reproduced from ref. 75 with permission from Wiley.) (c) *J*–*V* curves of blade-coated large-area F-PSMs with an active area of 100 cm^2.[77] (Reproduced from ref. 77 with permission from Wiley-VCH GmbH.) (d) *J*–*V* curve of the champion flexible PSC with an active area of 0.09 cm^2, along with the *J*–*V* curve of an F-PSM featuring an active area of 117.7 cm^2.[78] (Reproduced from ref. 78 with permission from the Royal Society of Chemistry.)

This journal is © The Royal Society of Chemistry 2025

Open Access Article. Published on 31 October 2025. Downloaded on 5/8/2026 2:03:17 PM.
This article is licensed under a Creative Commons Attribution 3.0 Unported Licence.

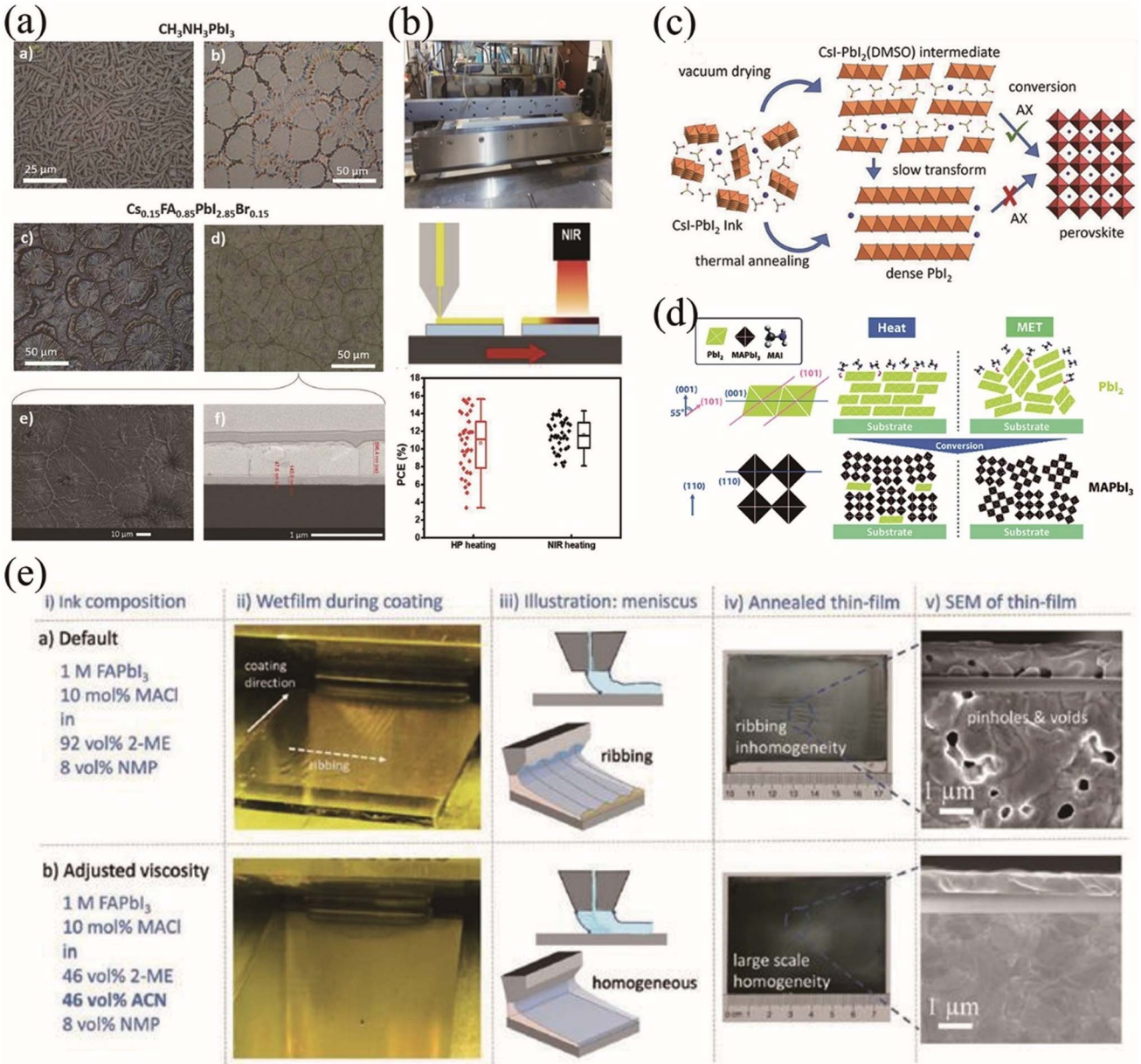

Fig. 6 (a) Microstructures of perovskite layers observed under an optical microscope, including $CH_3NH_3PbI_3$ layers dried at 140 °C using slow and fast temperature ramping, as well as $Cs_{0.15}FA_{0.85}PbI_{2.85}Br_{0.15}$ layers dried under similar conditions. The figure also includes an SEM image of the $Cs_{0.15}FA_{0.85}PbI_{2.85}Br_{0.15}$ layer processed with fast ramping, and a cross-sectional FIB-SEM image showing SnO_2 and perovskite layers coated on PET/ITO substrates.[84] (Reproduced from ref. 84 with permission from Wiley.) (b) Slot-die coating machine integrated with NIR heating, along with performance statistics of devices processed under different heating conditions.[86] (Reproduced from ref. 86 with permission from Wiley.) (c) Formation of a porous semi-amorphous CsI–PbI_2 (DMSO) precursor phase after vacuum drying the deposited CsI–PbI_2 ink. This structure is unstable and gradually converts into dense PbI_2 over time. In contrast, thermal annealing of the wet CsI–PbI_2 ink leads to the formation of highly crystalline, dense PbI_2, which, due to its compactness, cannot be completely converted into perovskite through slot-die coating.[88] (Reproduced from ref. 88 with permission from Wiley.) (d) Schematic comparison of the relative orientations of PbI_2 films fabricated by MET and conventional heat treatment, along with the corresponding $MAPbI_3$ films.[91] (Reproduced from ref. 91 with permission from the Royal Society of Chemistry.) (e) Comparison of thin-film homogeneity using two different precursor inks: 0% and 46% ACN in a 2-methoxyethanol (2-ME)/ACN mixed solvent. Column (ii) shows as-coated wet perovskite films; column (iii) presents schematic drawings of the meniscus and ribbing phenomena; column (iv) displays annealed film images; and column (v) includes SEM top-view and cross-sectional images of the perovskite films after annealing.[97] (Reproduced from ref. 97 with permission from Wiley.)

Open Access Article. Published on 31 October 2025. Downloaded on 5/8/2026 2:03:17 PM.
This article is licensed under a Creative Commons Attribution 3.0 Unported Licence.

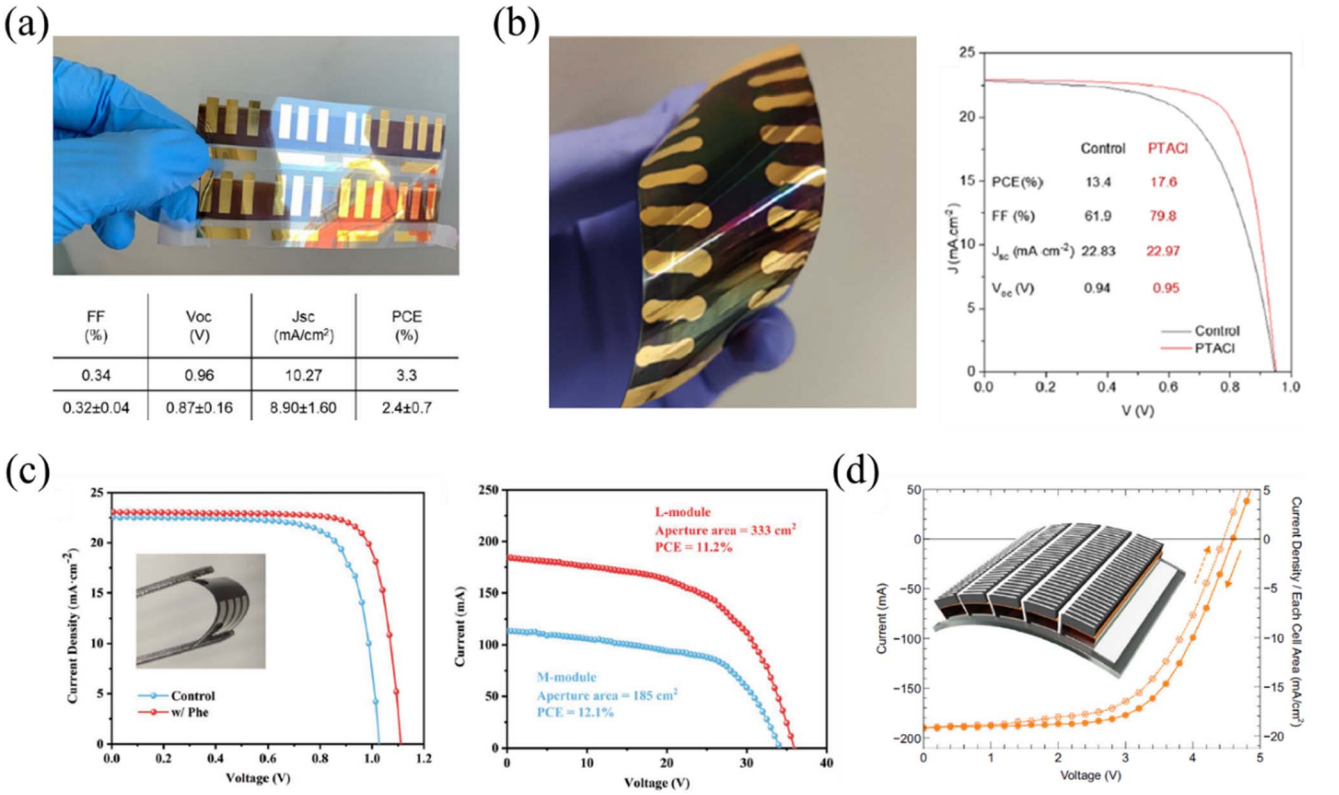

Fig. 7 (a) *J*–*V* characteristics of a fully slot-die coated device with a gold top electrode, fabricated and measured in an uncontrolled humid air environment (relative humidity: 65% and 75%). The best photovoltaic performance parameters and the average values obtained from 9 devices are shown.[99] (Reproduced from ref. 99 with permission from Wiley.) (b) Photograph of F-PSCs fabricated on a 3.25 cm × 7.5 cm substrate, each with 0.049 cm^2 active pixels, along with the *J*–*V* curve of the champion device.[102] (Reproduced from ref. 102 with permission from Wiley.) (c) Statistical distributions of photovoltaic parameters for F-PSCs with and without phenylethylammonium (PEA) additive.[103] (Reproduced from ref. 103 under CC BY 4.0, *Small Methods*, 2022.) (d) *J*–*V* curve of an R2R fabricated perovskite module. The inset shows a schematic diagram of the module structure.[104] (Reproduced from ref. 104 under CC BY 4.0, *Nature Communications*, 2024.)

This journal is © The Royal Society of Chemistry 2025

Open Access Article. Published on 31 October 2025. Downloaded on 5/8/2026 2:03:17 PM.
This article is licensed under a Creative Commons Attribution 3.0 Unported Licence.

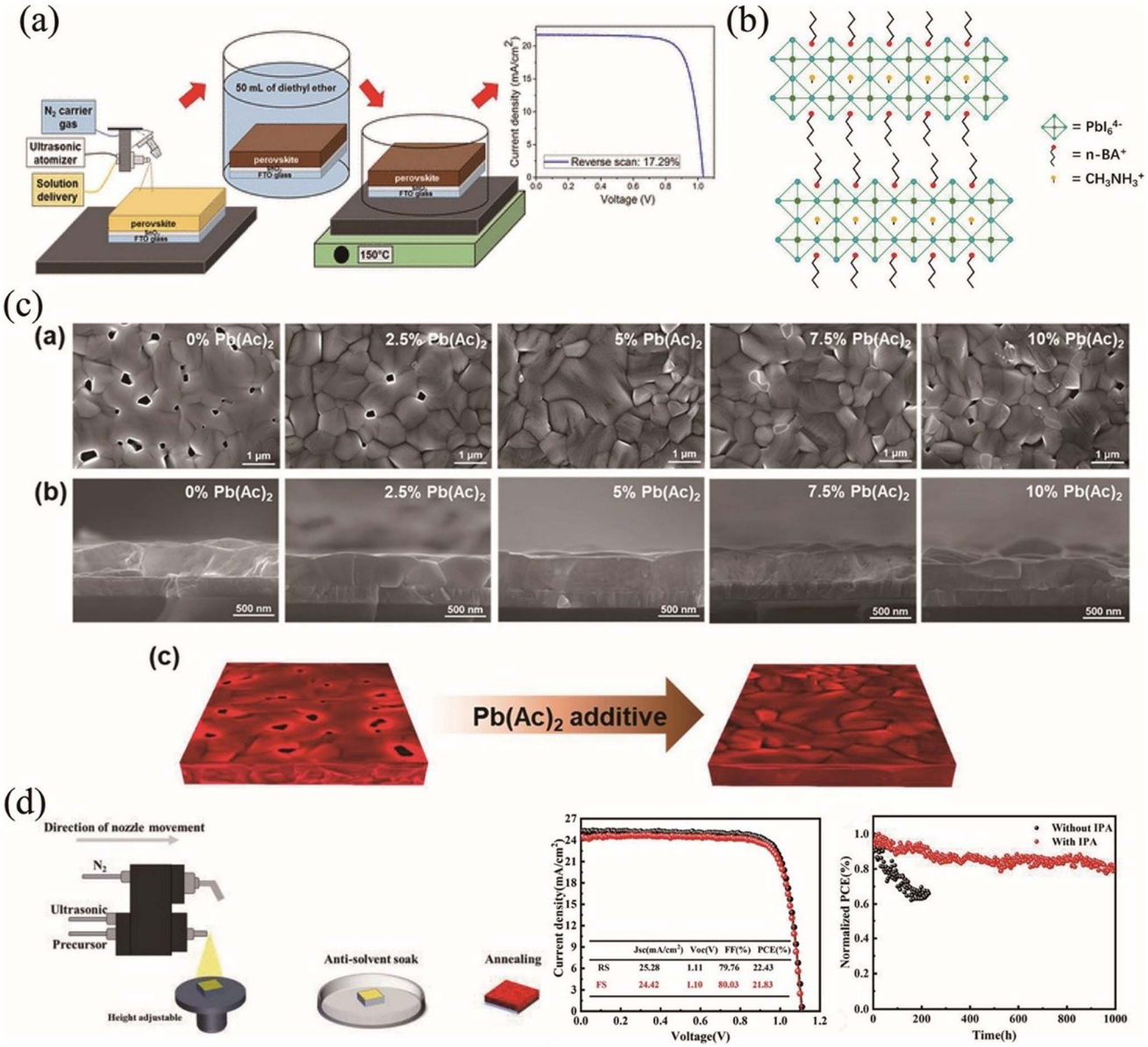

Fig. 8 (a) The use of a chlorine-containing perovskite ink with a broad processing window, combined with antisolvent extraction. This approach yielded perovskite films with relatively rougher surfaces compared to those produced by spin coating. The corresponding devices achieved a maximum PCE of 17.3%, with an average PCE of 16.3% across 24 devices.[112] (Reproduced from ref. 112 with permission from the American Chemical Society.) (b) The schematic crystal structure of the Ruddlesden–Popper phase $(BA)_2(MA)_3Pb_4I_{13}$.[115] (Reproduced from ref. 115 with permission from Elsevier.) (c) SEM images (top-view and cross-sectional) of spray-deposited $CsPbI_2Br$ perovskite films incorporating varying amounts of $Pb(Ac)_2$. A schematic comparison of $CsPbI_2Br$ films with and without the $Pb(Ac)_2$ additive is also provided.[120] (Reproduced from ref. 120 with permission from the American Chemical Society.) (d) A co-solvent strategy in which IPA is added to the perovskite precursor to modify the local microenvironment during ultrasonic spray coating (USC). The champion device achieved a PCE of 22.43% (active area: 0.13 cm^2) and retained 80% of its initial efficiency after 1000 hours of continuous illumination.[121] (Reproduced from ref. 121 with permission from Elsevier.)

Open Access Article. Published on 31 October 2025. Downloaded on 5/8/2026 2:03:17 PM.
This article is licensed under a Creative Commons Attribution 3.0 Unported Licence.

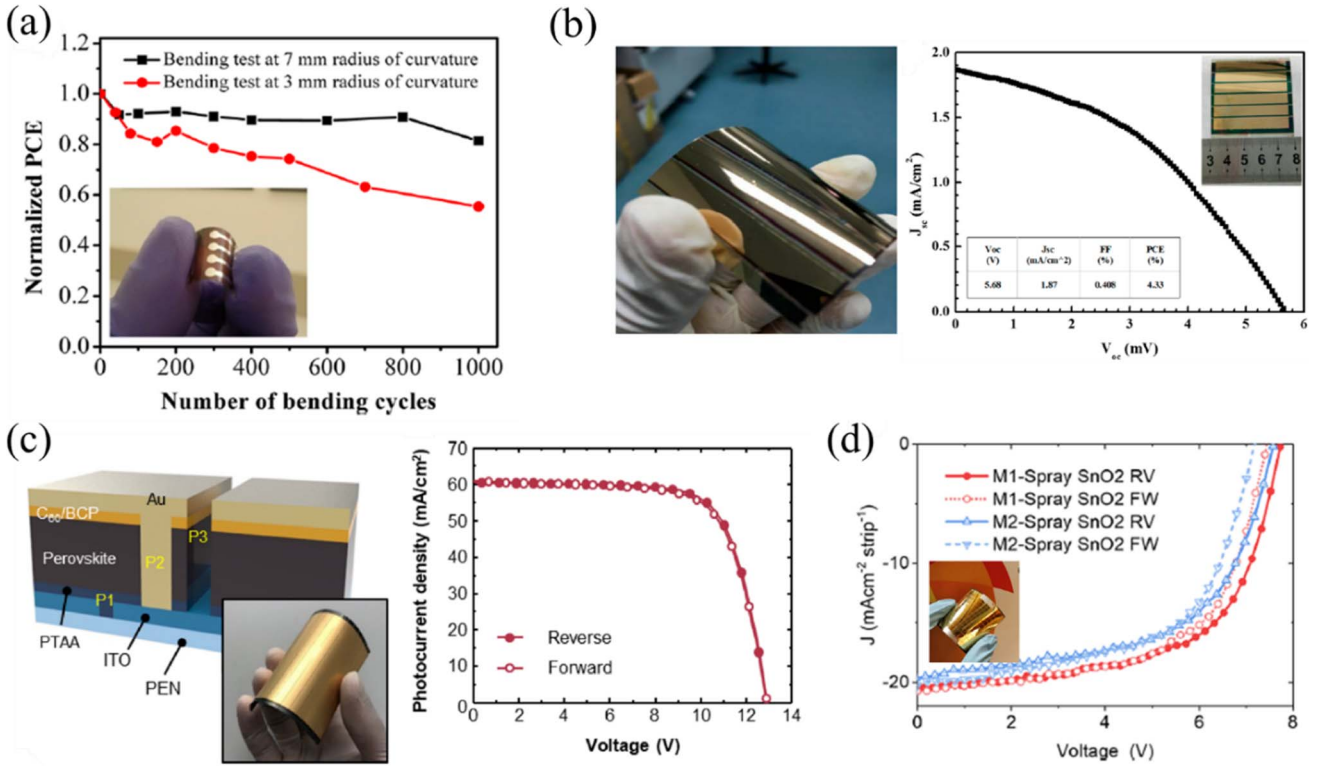

Fig. 9 (a) Normalized PCE of flexible devices after bending tests with radii of curvature of 7 mm and 3 mm. The inset shows a photographic image of the flexible devices.[106] (Reproduced from ref. 106 with permission from the American Chemical Society.) (b) Photographic image of a flexible device with a large area of 5.0 cm × 5.0 cm, along with the *J*–*V* characteristics of a typical F-PSC (active area: 13.5 cm^2) measured without a mask. The inset shows a typical F-PSM.[124] (Reproduced from ref. 124 under CC BY 4.0, *MDPI*, 2017.) (c) Schematic cross-sectional view and photograph of an F-PSM, accompanied by the *I*–*V* curves of a flexible perovskite mini-module with an active area of 35.1 cm^2.[125] (Reproduced from ref. 125 with permission from Springer Nature.) (d) *J*–*V* curves of an F-PSM fabricated with spray-coated SnO_2 films. The inset displays a photograph of the F-PSM.[127] (Reproduced from ref. 127 with permission from the American Chemical Society.)

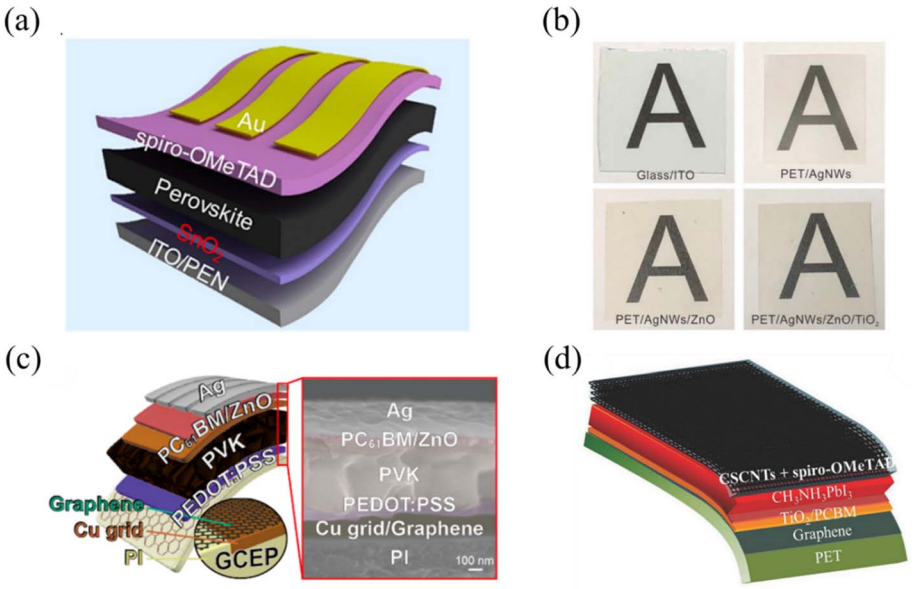

Fig. 10 (a) Schematic illustration of SnO_2-based flexible planar perovskite solar cells (SnO_2-F-PSCs).[150] (Reproduced from ref. 150 with permission from the American Chemical Society.) (b) Photographs comparing various flexible substrates with a conventional glass/ITO substrate.[158] (Reproduced from ref. 158 with permission from Wiley.) (c) Structure of F-PSCs employing an electrode platform composed of a conductive elastomeric polymer (CEP) film and graphene sheet (GCEP), along with the corresponding cross-sectional scanning electron microscopy (SEM) image.[159] (Reproduced from ref. 159 with permission from the American Chemical Society.) (d) Device architecture of flexible PSCs utilizing all-carbon electrodes.[171] (Reproduced from ref. 171 with permission from Wiley.)

This journal is © The Royal Society of Chemistry 2025

Open Access Article. Published on 31 October 2025. Downloaded on 5/8/2026 2:03:17 PM.
This article is licensed under a Creative Commons Attribution 3.0 Unported Licence.

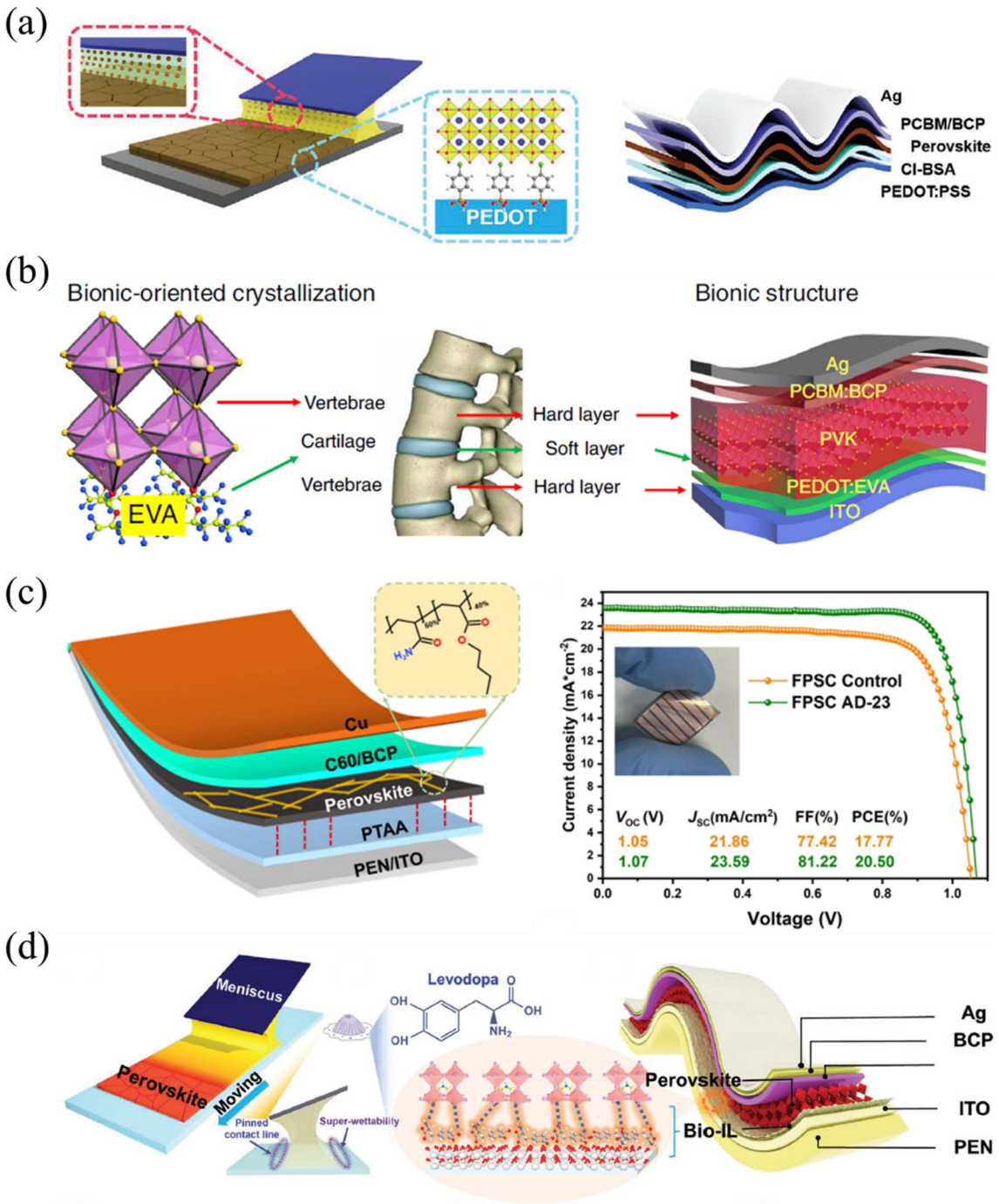

Fig. 11 (a) Schematic illustration of the nucleation, growth, and conversion processes involved in the fabrication of final F-PSCs.[175] (Reproduced from ref. 175 with permission from Wiley.) (b) Bioinspired structural concept showing the analogy between vertebrae and perovskite solar cells, emphasizing the application of nature-inspired design principles.[176] (Reproduced from ref. 176 under CC BY 4.0, *Nature Communications*, 2020.) (c) Device architecture of the F-PSC along with the corresponding *J*–*V* characteristics, illustrating its photovoltaic performance.[179] (Reproduced from ref. 179 with permission from Wiley.) (d) Schematic representation of the flexible printing process for PSCs, featuring a meniscus-guided blade-coating technique for perovskite film deposition at a blade speed of 5 mm s^{-1}, and the associated bio-inspired design and device structure of the printed PSC.[182] (Reproduced from ref. 182 with permission from Wiley-VCH GmbH.)

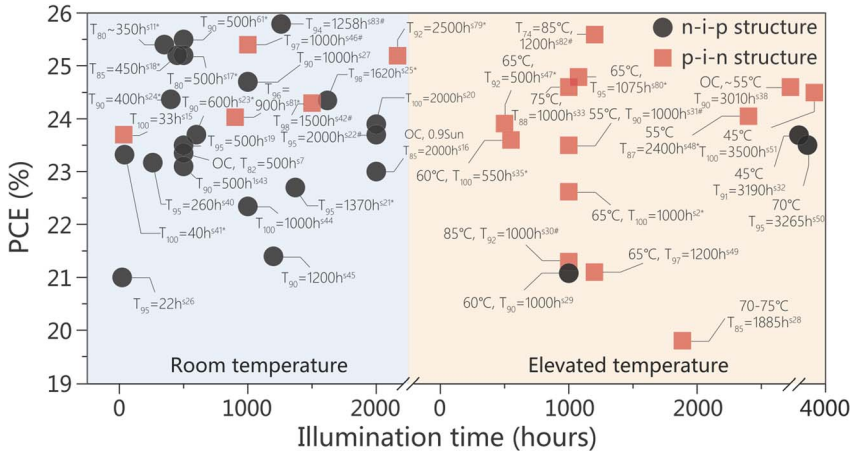

Fig. 13 The state of the art of perovskite stability under continuous illumination.[224] (Reproduced from ref. 224 with permission from Wiley-VCH GmbH.)

The Royal Society of Chemistry apologises for these errors and any consequent inconvenience to authors and readers.

Open Access Article. Published on 31 October 2025. Downloaded on 5/8/2026 2:03:17 PM.
This article is licensed under a Creative Commons Attribution 3.0 Unported Licence.

This journal is © The Royal Society of Chemistry 2025